



**HAL**  
open science

## Air quality, metal(loid) sources identification and environmental assessment using (bio)monitoring in the former mining district of Salsigne (Orbiel valley, France)

Aude Calas, Eva Schreck, Jérôme Viers, Astrid Avellan, Alain Pages, Maria Dias-Alves, Eric Gardrat, Philippe Behra, Véronique Pont

### ► To cite this version:

Aude Calas, Eva Schreck, Jérôme Viers, Astrid Avellan, Alain Pages, et al.. Air quality, metal(loid) sources identification and environmental assessment using (bio)monitoring in the former mining district of Salsigne (Orbiel valley, France). *Chemosphere*, 2024, 357, pp.141974. 10.1016/j.chemosphere.2024.141974 . hal-04579727

**HAL Id: hal-04579727**

**<https://hal.science/hal-04579727>**

Submitted on 18 May 2024

**HAL** is a multi-disciplinary open access archive for the deposit and dissemination of scientific research documents, whether they are published or not. The documents may come from teaching and research institutions in France or abroad, or from public or private research centers.

L'archive ouverte pluridisciplinaire **HAL**, est destinée au dépôt et à la diffusion de documents scientifiques de niveau recherche, publiés ou non, émanant des établissements d'enseignement et de recherche français ou étrangers, des laboratoires publics ou privés.



26 Active monitors (particulate matter samplers) and passive bioindicators (*Tillandsia usneoides*) were  
27 placed in strategic sites including remote areas. Over the year 2022, we assessed the air quality using  
28 microscopic and spectroscopic techniques, as well as environmental risk indicators to report the level  
29 of contamination.

30 Results indicate that the overall air quality in the valley is good with PM<sub>10</sub> levels in accordance with EU  
31 standards. Elemental concentrations in the exposed plants were lower than reported in the literature.  
32 Among the different sites studied, Nartau and La Combe du Saut, corresponding to waste storage and  
33 former mining industry sites, were the most affected. Chronic exposure over 1 year was highlighted  
34 for Fe, Ni, Cu, Pb, Sb and As. Pollution Load Index and Enrichment Factors, which provided valuable  
35 information to assess the environmental condition of the valley's air, suggested that dust and  
36 resuspension of anthropogenic materials were the principle sources for most of the elements. Finally,  
37 this study also highlights that using *T. usneoides* could be a convenient approach for biomonitoring of  
38 metal(loid)-rich particles in the atmosphere within a former mining area, for at least one year. These  
39 results in turn allow to better understand the effects of chronic exposure on the ecosystem.

40

#### 41 **Highlights**

- 42 - In 2022, the Orbiel valley air quality was in compliance with regulations
- 43 - Dust and anthropogenic resuspensions were the principal sources of metal(loid)s
- 44 - NRT and CDS sites were identified to be the most contaminated sites
- 45 - Except Cu and Zn, all elements showed linear deposition kinetics on *T. usneoides*

46

47

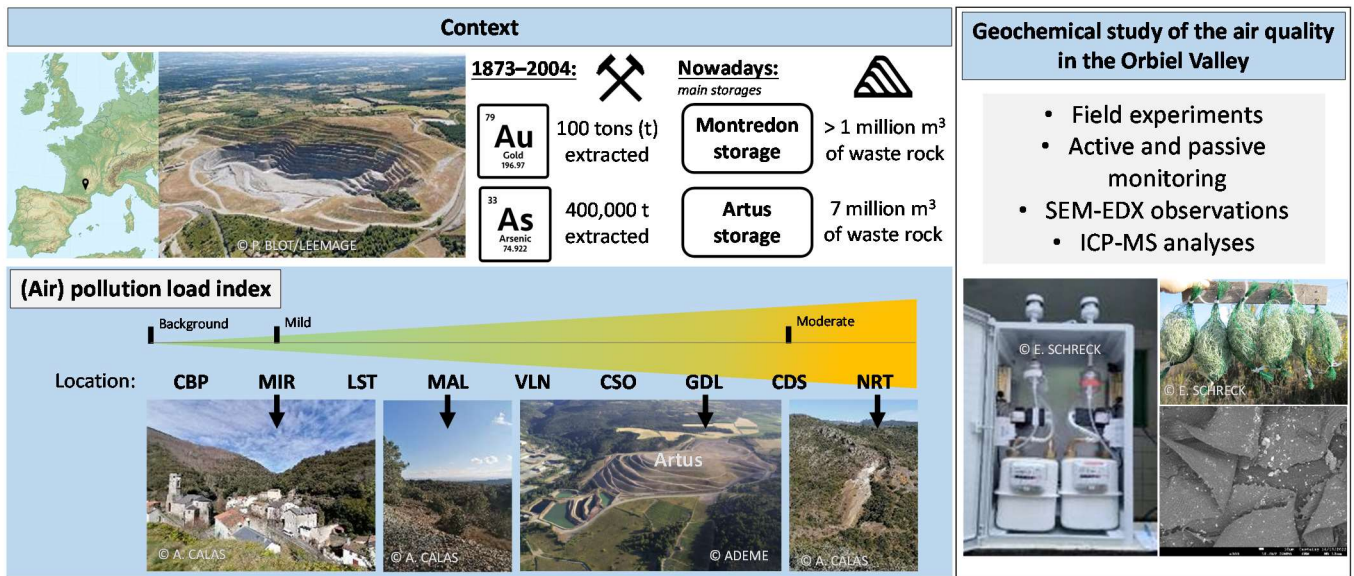
48

49

50

51

52 Graphical Abstract



53

## 54 1. Introduction

55 Mining activities contribute significantly to toxic metal(loid) contaminants in the environment, which  
56 persist long (even decades) after mine closure (Delplace et al., 2022). The different environmental  
57 components, i.e., surface and groundwater, soil, sediment, atmosphere and biosphere, typically bear  
58 this impact (Bondu et al., 2023; Chen et al., 2017; Delplace et al., 2022; Elbaz-Poulichet et al., 2017;  
59 Huertas et al., 2012; Tepanosyan et al., 2018). In southern France, the border region of the Massif  
60 Central has long served as a major mining area for non-ferrous (Pb-Zn-Ag-Au) metals dating back to at  
61 least the medieval period and probably even as early as the Roman period (Elbaz-Poulichet et al.,  
62 2017). In the late 19<sup>th</sup> century, following the discovery of Au ores, mining activities were intensified  
63 and continued up until the second half of the 20<sup>th</sup> century, after which they gradually decreased (Elbaz-  
64 Poulichet et al., 2017). Located on the south-western terminus of the Massif Central area, the Orbiel  
65 valley, more precisely, the Salsigne old mining district, includes various sites that are linked to former  
66 (ore extraction and processing) and current mining activities (waste storage). The main mine was, at  
67 some point in the 20<sup>th</sup> century, the first Au mine in Europe and the first As mine in the world. In the  
68 period following the discovery of Au in 1892 until the closure of the mine in 2004, around 120 t of Au  
69 were produced, the highest output of any Au mine in Western Europe. From 1873 to 1910, about 25%  
70 of the world's As needs were supplied by this mine (Drouhot et al., 2014; Trueb, 1996). However, as  
71 indicated by the various mining concessions, there were several other secondary mines in this area  
72 (Figure 1 top map), covering a total surface area of 39.78 km<sup>2</sup> (Vermeersch et al., 2012). Ore  
73 processing, which historically was conducted close to the extraction sites, was later relocated to the  
74 central processing area of La Combe du Saut (Desaulty et al., 2016). After the closure of the different  
75 mines and factories, a rehabilitation of the area was undertaken and carried out over a span of 20  
76 years with several million t of waste stored in the valley. The main waste storages are located at the  
77 sites of Montredon (> 1 million m<sup>3</sup> of waste rock), Artus (7 million m<sup>3</sup> of waste rock), and La Combe du  
78 Saut (Rochereau et al., 2021). The Montredon storage (MRD) area, while mainly containing waste from  
79 the cyanidation of ores, also has flotation residues, lime arsenates, residues from the Malabau

80 concession, and sewage sludge. The Artus storage (ART) area also serves as a repository for waste from  
81 the cyanidation of the ore and flotation residues but unlike Montredon, this storage site neither has a  
82 bottom seal nor does it have a waterproof covering system (Desaulty et al., 2016). Finally, the wastes  
83 produced from the demolition of factory buildings and pyrometallurgical slag are the main wastes  
84 stored in geomembranes at La Combe du Saut (CDS) (Desaulty et al., 2016; Drouhot et al., 2014). Other  
85 waste rock piles located in the valley include the waste pile of Nartau (NRT), the waste pile of Malabau  
86 (MAL) (45 000 m<sup>3</sup>), (Vermeersch et al., 2012), the waste storage of La Caunette (CAU), or the waste  
87 piles surrounding the open-mine of Salsigne (SAL, RML) (Figure 1).

88 The most recent extreme precipitations and flood events, (October 2018, categorized as a 100-year  
89 flood) have brought to light the mining history of the area and have raised concerns among a certain  
90 segment of the inhabitants in the valley regarding their immediate environment.

91 Recent studies have revealed the contamination by metals and metalloids, particularly of As, due to  
92 anthropogenic activities, of surface and groundwaters (Heydon et al., 2023; Khaska et al., 2015),  
93 sediments (Delplace et al., 2022), and also As transfer to wild small mammals (Drouhot et al., 2014).

94 Furthermore, since 1997, prefectural decrees, starting with the publication of the first decree  
95 concerning vegetable sales, have been issued, prohibiting the sale of certain vegetables grown in the  
96 Orbiel valley or the utilization of water from the Orbiel river and its tributaries. However, despite  
97 numerous studies on the various environmental components, there have been only few studies on the  
98 levels of atmospheric pollution in this impacted valley (Bausch and Merlen, 2021; Durif et al., 2006).  
99 This is all the more relevant because, the World Health Organization (WHO) has estimated that every  
100 year, exposure to ambient air pollution causes millions of deaths and the loss of healthy years of life  
101 (World Health Organization, 2021). In the past, mining activities were assumed to be major sources of  
102 toxic elements such as As in the atmosphere, in the form of aerosols and gas, from the mine and the  
103 extraction plants in the Orbiel valley. It is noted here that there have been no peer-reviewed studies  
104 to assess air quality in this rural and windy valley since mining operations ceased. There are however,  
105 two technical reports by the French Geological Survey (BRGM), responsible for the rehabilitation of

106 the mining sites of the area (Bausch and Merlen, 2021; Durif et al., 2006). The valley has a typically  
107 continental climate with a blend of Mediterranean and oceanic influences featuring a relatively high  
108 annual rainfall (900 mm) combined with a mild annual average temperature (13 °C) (Delplace et al.,  
109 2022). Additionally, the valley also frequently experiences strong winds (average values in Carcassonne  
110 from 1991 to 2022: 98.5 d/y with wind speed > 16 m/s). Moreover, wind friction on surfaces such as  
111 the waste storage sites, has already been reported to contribute significantly to the emission and  
112 transport of metal(loid)-rich particles in mining areas. The potential impacts of these emissions on the  
113 environment and human health have been described (Blondet et al., 2019; Csavina et al. 2012; Sánchez  
114 de la Campa et al., 2011; Yulevitch et al., 2020; Zota et al., 2009).

115 In addition to traditionally used methods, several new approaches such as biomonitoring have been  
116 developed in recent years to monitor atmospheric quality. Biomonitoring methods include the use of  
117 bioindicators such as mosses, lichens, tree barks, tree rings, pine needles, grass, leaves and ferns  
118 (Figueiredo et al., 2007) but also the use of epiphytic bromeliads (i.e., *Tillandsia spp.*) that absorb water  
119 and nutrients directly from the atmosphere and are adapted to avoid hydric stress. These low-cost and  
120 easy-to-perform tools help to overcome technical constraints associated with field studies, such as lack  
121 of electricity or areas that do not have easy access, and to better assess air quality over larger and  
122 more remote areas. Among the *Tillandsia spp.*, *Tillandsia usneoides* has been reported to be a good  
123 bioindicator to detect metal contamination (Figueiredo et al., 2007; Isaac-Olivé et al., 2012; Martínez-  
124 Carrillo et al., 2010; Parente et al., 2023; Pellegrini et al., 2014; Schreck et al., 2020) and to identify the  
125 sources of contamination (dust, vehicular, industrial origin) (Figueiredo et al., 2007; Pellegrini et al.,  
126 2014) as reported in several recent studies, especially in South America. In these studies, the  
127 consecutive monitoring periods ranged from 15 days (Isaac-Olivé et al., 2012; Martínez-Carrillo et al.,  
128 2010) to 52 weeks (Schreck at al., 2020) but were usually shorter than 13 weeks. Notwithstanding, *T.*  
129 *usneoides* has rarely been used in Europe (Pellegrini et al., 2014; Schreck at al. 2020).

130 In this study, we conducted field experiments using active monitors such as PM samplers, while  
131 complementing them with passive bioindicators, specifically *T. usneoides*, in order to (i) assess the air

132 quality of the Orbiel valley over a one-year time period using traditional PM samplers as well as  
133 innovative plants-based tools in the more remote areas, (ii) identify potential sources of air  
134 contamination as well as the most impacted areas in the valley, (iii) assess the environmental status of  
135 the valley using pollution indexes from an atmospheric standpoint.

## 136 2. Material and methods

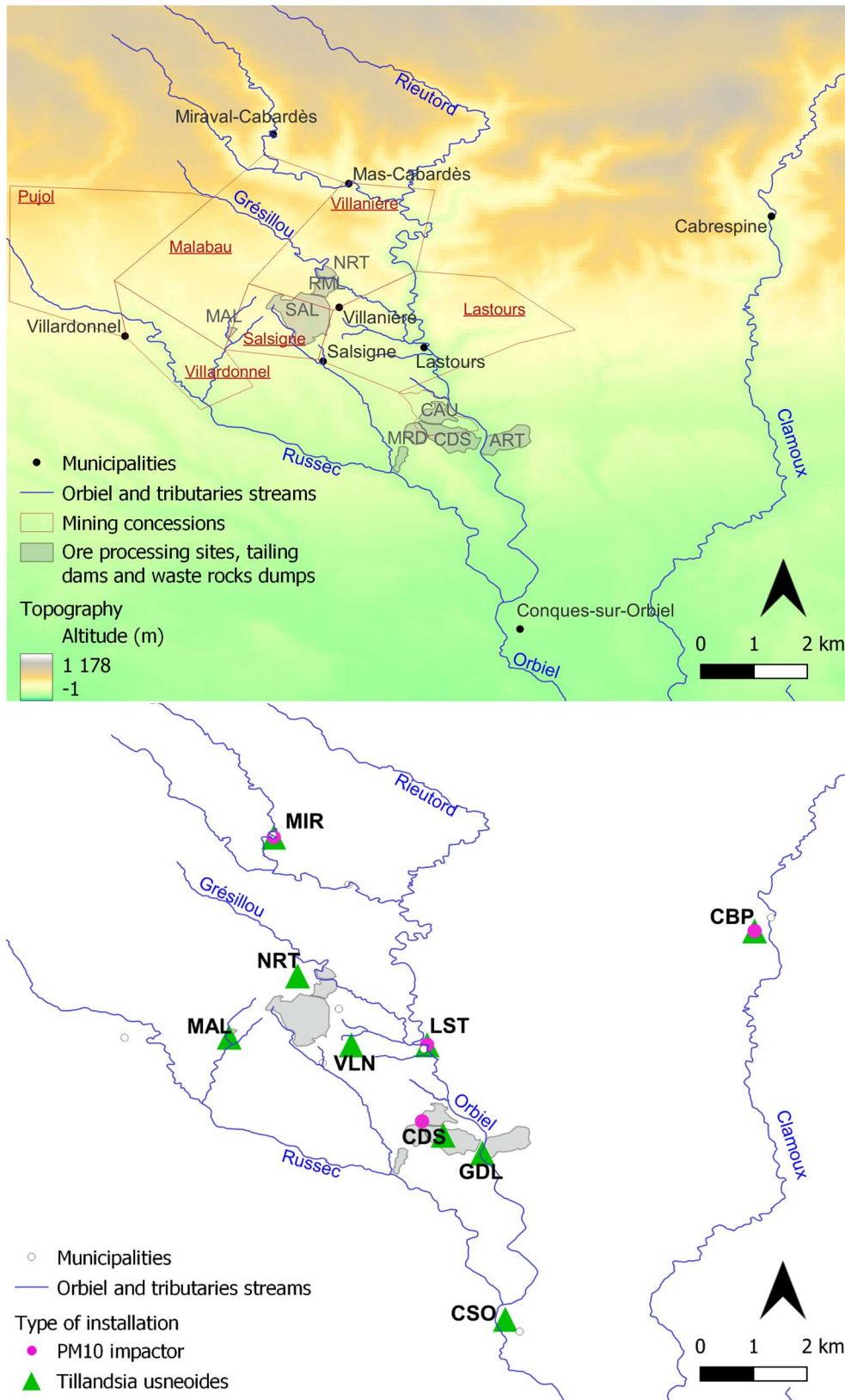
### 137 2.1. Study area and instrumentation

138 The main waste storage areas, namely, Montredon (MRD), La combe du Saut (CDS), and Artus (ART)  
139 are located in the villages of Salsigne, Lastours and Limousis, respectively, and situated at around 13  
140 Km north of the city of Carcassonne (South France, Figure 1).

141 We selected nine strategic sites to assess the overall air quality in the selected area (Figure 1 bottom  
142 map, Table SI 1). Passive bioindicators such as *T.usneoides*, as well as the active monitors, PM<sub>10</sub>  
143 collected on Teflon filters, were deployed in 4 sites: The **Gouffre de Cabrespine (CBP** – the control site  
144 without any past mining exploitation activity and located in the Clamoux valley), **Miraval-Cabardès**  
145 (**MIR** – a village in the upstream part of the Orbiel river characterized by minimal mining activities),  
146 **Lastours (LST** – another village situated downstream along the river and containing several mine  
147 galleries), and **La Combe du Saut (CDS** – formerly the main ore processing area but now mainly  
148 containing waste from the demolition of the plant buildings). The last site is also in proximity to La  
149 Caunette (CAU), a former ore processing and storage area, and the waste storage facility of Montredon  
150 (MRD). Today, “La Caunette” corresponds to an open quarry for aggregates located in the CAU  
151 concession.

152 Passive biomonitoring was extended to 5 sites, which allowed to better cover the valley and extend  
153 the study to rural areas and more remote sites such as, **Conques-sur-Orbiel (CSO** – town in the  
154 downstream part of the Orbiel river and without past mining activities), **Villanière (VLN** - 300 m from  
155 the waste rock pile of Cimetière south of the open-pit mine of Salsigne (SAL) and in proximity to the  
156 town of Villanière), **Malabau (MAL** – on the waste rock pile, a former ore extraction and processing  
157 site), **Nartau (NRT** –500 m from the waste rock pile of Nartau (NRT), a former ore extraction and  
158 processing site and at 600 m from the waste rock pile of Terrisse/Ramèle (RML) situated north-east of  
159 the open-pit mine of Salsigne (SAL), and **Gué de Lassac (GDL** - near the storage facility of Artus (ART)).

160 From the sites of MIR (north), to MAL (west), to CSO (south), to LST (east), the (bio)monitoring area  
161 represents 22 km<sup>2</sup>, excluding the control site of CBP, in the Clamoux valley.



162

163 Figure 1: General context and sampling strategy. *Top map*: mining history of the Orbiel valley with topographic description.

164 *Bottom map*: location of the sampling sites for atmospheric (bio)monitoring from October 2021 to December 2022, in the

165 Orbiel valley (Aude, France); CBP = Gouffre de Cabrespine; MIR = Miraval; CSO = La Conques sur Orbiel; LST= Lastours; VLN =

166 Villanière; MAL = Malabau; NRT = Nartau; GDL = Gué de Lassac; CDS = La Combe du Saut.

## 167 2.2. Abiotic parameters

168 Recordings of abiotic parameters, i.e. wind and precipitation, were used to better understand their  
169 influence on PM<sub>10</sub> distribution in the environment. Synoptic wind variables, i.e. wind direction and  
170 speed at GPS point 43°20'52" N, 2°23'29" E, were extracted from *earth.nullschool.net*, based on  
171 forecasts and reanalysis from the Global Forecast System (GFS, EMC / NCEP / US National Weather  
172 Service). These data can be used to track large-scale atmospheric flows and were extracted daily at  
173 12h00 and 700 hPa altitude. The wind direction most frequently observed over a period of 15 days was  
174 selected to represent the direction of maximum influence over the 15-integrated days of PM<sub>10</sub>  
175 sampling. The median wind speed was calculated over the same 15-day period.

176 With regard to precipitation, the Integrated Multi-satellite Retrievals algorithm of the international  
177 satellite mission Global Precipitation Measurement (GPM) was used to estimate precipitation in the  
178 Orbiel valley. The data were provided by Google Earth Engine, through the GPM v6 collection with a  
179 spatial resolution of 0.1°× 0.1° (roughly 10 km x 10 km) and a temporal resolution of 30 min (as used  
180 by de Fleury et al., 2023). The cumulative amount of precipitation was also calculated over the same  
181 15-day period.

182

## 183 2.3. Experimental set-up and sampling

### 184 2.3.1. PM<sub>10</sub> sampling for air composition study

185 Our choice to study PM<sub>10</sub> was based on the fact that coarse particles were expected to be associated  
186 with waste storage areas, i.e. plant closure, potential particle emissions due to wind friction on  
187 surfaces. In December 2021, we installed PM<sub>10</sub> impactors in 4 sites (see Figure 1 and Table SI 1).  
188 Aerosols were collected continuously on Teflon filters during 15-integrated sampling days, in the time  
189 period from December 2021 to December 2022. The PM<sub>10</sub> impactors operated at a flow rate of 5 L min<sup>-1</sup>.  
190 <sup>1</sup>. Samples of PM<sub>10</sub> were collected on Teflon filters (Pall TF-45, 47 mm diameter and 0.45 µm cut off) to

191 characterise particulate trace metals and metalloids of interest. Teflon filters, including blanks, were  
192 weighed before and after sampling, and analysed for trace elements. Note that for the CDS site,  
193 sampling started 2 weeks after sampling in the other sites (January 2022).

194

### 195 2.3.2. Experimental set-up using *T. usneoides* as indicator to determine 196 metal(loid) concentrations in the air

197 Plants of similar size were bought at Botanic® garden supplies store and washed with ultrapure water.  
198 The plants were then placed in nylon mesh bags containing one plant in each bag (Figure SI 1). In  
199 October 2021, in each of the 9 sites, 6 bags per site were secured on trees or wooden posts at a height  
200 of 1.7 m. At each of the sites, a plant was collected every 2 months in the time period between January  
201 and November 2022 to determine the kinetics of deposition (and potential uptake) of airborne  
202 particulate matter over a full year. After collection, the plants were dried at 45 °C for 48 – 72 h, ground  
203 in an agate mortar with liquid N<sub>2</sub>, dried again if needed, and stored in polyethylene vials.  
204 Additionally, 3 nylon mesh bags (containing 3 *T. usneoides*) were kept in the laboratory as controls  
205 (unexposed) in October 2021. In November 2021, these controls were dried, ground and analysed in  
206 an identical manner as the exposed *T. usneoides* samples. Following the methodology of Figueiredo et  
207 al. (2007), the plants were not washed after exposure because both deposition and potential uptake  
208 are considered in this study.

209

### 210 2.4. SEM-EDX observations of epiphytic plants

211 Environmental scanning electron microscopy with energy-dispersive X-ray spectroscopy (SEM-EDX)  
212 measurements were carried out on epiphytic plants at the Centre de Microcaractérisation Raimond  
213 Castaing in Toulouse (France), using a (FEG) JSM-7800F Prime (Jeol®) instrument equipped with EDX  
214 detector. SEM-EDX analyses were performed on unwashed *T. usneoides* exposed for 6 months in CDS,

215 to observe their morphology, trichome conformation, and the possible presence of metal(loid)s on the  
216 plant surface. Plants were dried and fixed on a carbon substrate and imaged as such.

217

## 218 2.5. Acidic mineralisation of samples and determination of elemental 219 concentrations by ICP-MS

220 To determine the elemental composition of *T. usneoides*, 0.100 g of dry matter was digested using a  
221 mixture of 8 mL of bi-distilled HNO<sub>3</sub> and 2 mL HF (suprapure quality). Acid mineralisation was  
222 conducted using a CEM® Mars 6 microwave with iPrep vessels using the program “plant tissue”. The  
223 heating protocol consisted of a 30 min ramp to 200 °C followed by a holding time of 10 min before  
224 cooling.

225 For the collected PM<sub>10</sub> samples, half of the Teflon filter (previously weighed) was used and the PM<sub>10</sub>  
226 were digested using the same acid mixture as for the plants. In this case, the “filter membrane”  
227 program was used, which consisted of a 30 min ramp until 200 °C followed by a holding time of 15 min  
228 before cooling.

229 All the obtained solutions were evaporated at 70 °C on a hotplate and the dry residues were  
230 resuspended in 0.37 N HNO<sub>3</sub> before analysis. Metal and metalloid concentrations in all diluted  
231 solutions (HNO<sub>3</sub> 0.37N) were determined using inductively coupled plasma-mass spectrometry (ICP-  
232 MS) (iCAP Q Thermo Scientific®, from the ICP-MS Service of the Midi-Pyrénées Observatory in  
233 Toulouse, spiked with an In-Re internal standard to correct for instrumental drifts and plasma  
234 fluctuations; and from the ICP-MS AETE-ISO platform of OSU OREME, at the University of Montpellier,  
235 using Be, Sc, Ge, Rh and Ir as internal standards). Each batch of samples included an acid blank (or filter  
236 blank) and a certified reference material: SRM 1515 Apple leaves from the National Institute of  
237 Standards and Technology (NIST, USA) for *T. usneoides* samples and, SRM 1648a Urban particulate  
238 matter (NIST, USA) for the PM<sub>10</sub> samples. Details on the quality of acid mineralisation, i.e. recoveries  
239 for the elements of SRM 1515 and SRM 1648a, are given in Supplementary Information (Table SI 2).

240 Details on the quality of the instrumental analyses, i.e. limits of detection (LOD) calculated as the  
241 average plus 3 times the standard deviation (SD) of the concentrations in the HNO<sub>3</sub> blanks, and  
242 recoveries for the elements of the instrumental SRMs: SRLS-6 (river water certified reference material  
243 for trace metals and other constituents) and EPOND (multi-element standard solution) are also given  
244 in Supplementary Information (Tables SI 3 and SI 4, respectively).

245

## 246 2.6. Atmospheric fallouts sourcing and environmental risk assessment

247 Enrichment factors (EF) and the pollution load index (PLI) were calculated to allow sources  
248 identification and risk assessment for the environment. In this study, the enrichment factors were  
249 considered to be indicative of the relative contribution of rock and soil dust to the elemental  
250 composition of *T. usneoides*. This is in view of the fact that emission of particles could potentially occur  
251 due to wind friction on surfaces. Enrichment factors were then calculated for each element by  
252 comparing their concentrations with the average upper crust (UC) composition reported by Rudnick  
253 and Gao (2003). Titanium (Ti) was chosen as the invariant for normalisation. This assumption is in  
254 accordance with the previous work by Delplace et al. (2022) who showed that the Ti content in the  
255 soils and sediments of the Orbiel valley has remained constant, with a  $Ti/Ti_{upper\ crust}$  ratio close to  
256 1. EF were calculated according to the formula:

$$257 EF = (Ci/CTi_{Tillandsia}) \div (Ci/CTi_{UC})$$

258 where  $Ci$  is the measured metal(loid) concentration, and  $CTi$  is the Ti concentration in the *T. usneoides*  
259 sample or in the upper crust (UC) (Pellegrini et al., 2014). In this study, EF values up to 10 are  
260 interpreted as indicative of a natural local dust origin from rock and soil, whereas higher EF values  
261 suggest input from sources other than rock and soil dust, potentially of anthropogenic origin. It should  
262 be noted that in EF calculations, the metal(loid) concentration (averaged over several specimens) in  
263 the unexposed plants was subtracted from the obtained concentration in the exposed plants. Even if  
264 the cut off value could be debated (Reimann and de Caritat (2005)), elements with  $EF > 10$  are generally

265 considered to be enriched relative to their crustal abundances, and those with EF < 10 are considered  
266 non-enriched, as defined by Rahn (1976). This arbitrary cut off has been widely used by various authors  
267 including Dasch and Wolff (1989), Esmailirad et al. (2020), Freydier and Viers (2003), Gerdol et al.  
268 (2000), Pellegrini et al. (2004) and Veysseyre et al. (2001).

269 Finally, the PLI indicates the contribution of each metal(loid) to the global contamination of an area.  
270 The PLI, first proposed by Tomlinson et al. (1980) and recently used by Chen et al. (2022), was used to  
271 assess the environmental status of the different locations monitored by epiphytic plants. It was  
272 calculated by the following relationships:

$$273 \quad P_i = C_i \div C_n^i$$
$$274 \quad PLI = \sqrt[n]{\prod_i P_i}$$

275 where  $P_i$  is the single-factor pollution index,  $C_i$  are the measured metal(loid) concentrations in the  
276 exposed *T. usneoides* of the Orbiel valley, and  $C_n^i$  are the measured metal(loid) concentrations in the  
277 plants of control site of CBP for each of the exposure periods. According to the classification of Chen  
278 et al. (2022), the PLI values were then ranked in four levels, indicating no (PLI <1), mild (1 = PLI <2),  
279 moderate (2 = PLI <3), and severe pollution (PLI ≥3).

280

## 281 2.7. Statistical analyses

282 Statistical analyses were carried out using the R statistical software® 4.1.3. Given the size of the dataset  
283 and/or the non-normal distribution of the data, we used non-parametric Mann-Whitney tests to  
284 evaluate the statistical significance between the 9 exposure sites and the 4 exposure seasons. Non-  
285 parametric Spearman's rank correlations (denoted as R) were utilized to evaluate the strength of  
286 possible monotonic relationships between the different influencing factors, i.e., between elements  
287 and abiotic parameters, or between elements and the exposure time. P-values <0.05 were considered  
288 as statistically significant. Finally, PCA was done using the FactorMineR® package. Since the variables

289 were scaled in the PCA, replacing the missing data (values < LOD, representing 4 out of 60 values for  
290 the Tillandsia dataset and 6 out of 95 values for the PM<sub>10</sub> dataset) by the average of the corresponding  
291 variables (for each specific location) should have no effect on PCA results. It should be noted that the  
292 results however, could be affected by outliers, since the PCA from FactoMineR is based on the  
293 Pearson's correlation coefficient matrix.

294

### 295 3. Results

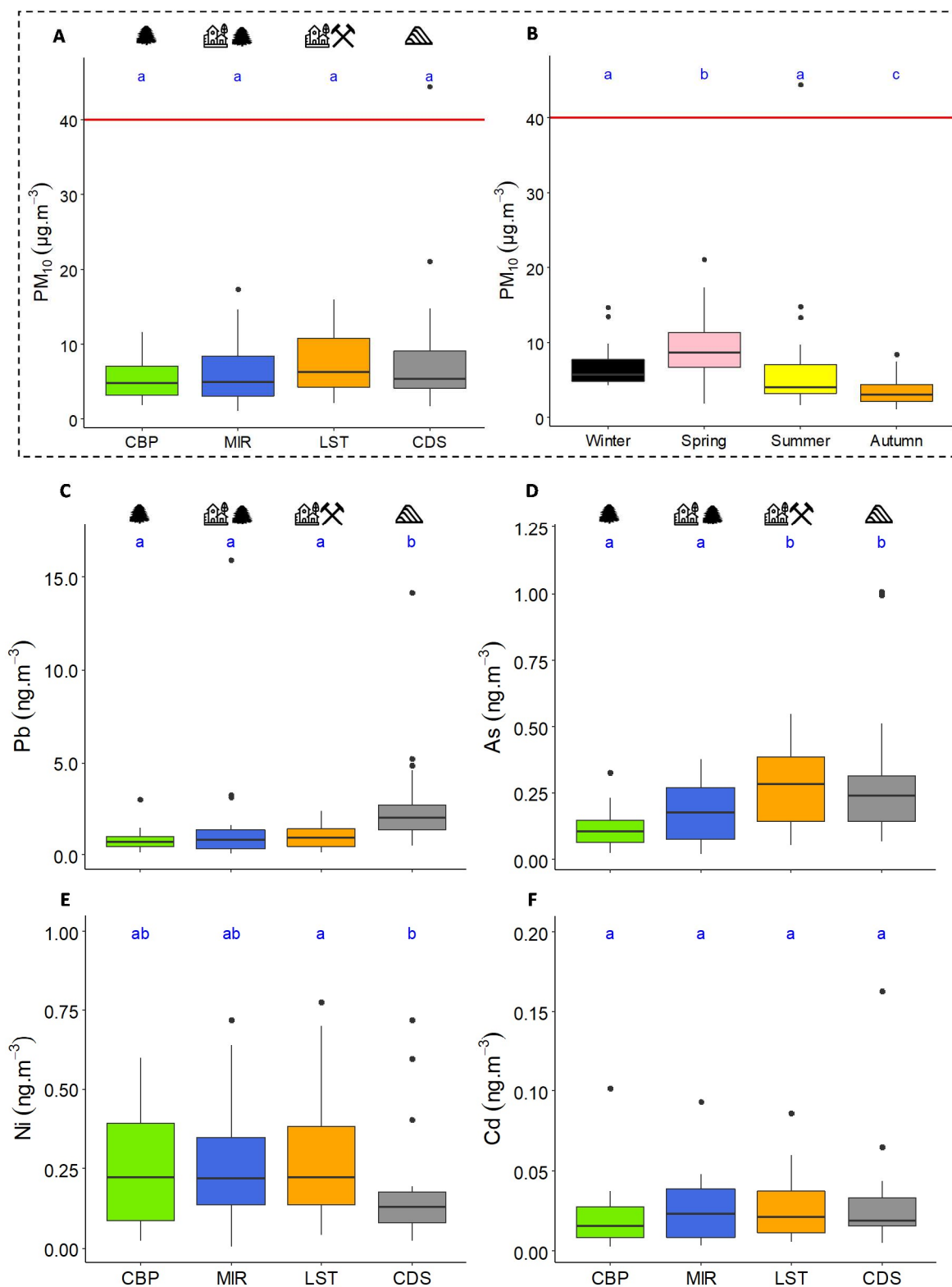
296 In this study, we chose nine elements for analysis. Pb, As, Ni, Cd were investigated in view of their  
297 relevance to air quality standards regulations. In addition, we included elements that are indicative  
298 markers for different pollution sources such as dust (Ti, Fe), vehicle emissions (Cu, Sb, Cd), industrial  
299 activities (As, Cd, Pb, Zn), and fuel oil combustion (Ni) (Esmailirad et al. (2020)).

300

#### 301 3.1. PM<sub>10</sub> characterisation: mass concentration and elemental composition

302 The annual mass concentration values for PM<sub>10</sub> collected in the Orbiel valley from Dec. 2021 to Dec.  
303 2022 are reported in Figure 2 (A & B). It is seen that these values meet the European air quality  
304 standards (annual average 40 µg.m<sup>-3</sup>) and there is no significant difference between the 4 sites. The  
305 average values for PM<sub>10</sub> mass concentration are: 5.4, 6.1, 7.5 and 8.4 µg.m<sup>-3</sup> in CBP, MIR, LST and CDS,  
306 respectively. Moreover, the concentration in PM<sub>10</sub>, all sites combined, was significantly higher in spring  
307 and lower in autumn 2022 (Figure 2 - B).

308



309

310 Figure 2: Mass concentrations of PM<sub>10</sub> and of the metal(loid)s content in PM<sub>10</sub> at the different investigated sites and over  
 311 different seasons. *Top figures*: Annual PM<sub>10</sub> mass concentrations (A) and seasonal distribution (B) of the PM<sub>10</sub> concentrations  
 312 (for all sites combined). *Bottom figures*: Elemental composition of Pb (C), As (D), Ni (E) and Cd (F). *Sites*: CBP = Gouffre de  
 313 Cabrespine, MIR = Miraval, LST = Lastours, CDS = La Combe du Saut. *Red line* = PM<sub>10</sub> European air quality standards. *Blue*  
 314 *letters represent the statistical difference between sites or seasons (non-parametric Mann-Whitney tests).*

315 Data from PM<sub>10</sub> impactors show that the annual mass concentration values for Pb, As, Ni and Cd meet  
316 the European air quality standards of 500, 6, 20 and 5 ng.m<sup>-3</sup>, respectively (Figure 2 – C, D, E & F). Some  
317 differences were observed between the different sites for all elements except for Cd, which had a very  
318 low mass concentration in all the sites (average values of 0.02 in Gouffre de Cabrespine (CBP) to 0.03  
319 ng.m<sup>-3</sup> for the other sites). For Pb, the mass concentration was significantly higher in La Combe du Saut  
320 site (CDS – average value of 2.8 ng.m<sup>-3</sup>) than in the other sites (0.80 ng.m<sup>-3</sup> in CBP, 1.5 ng.m<sup>-3</sup> in Miraval  
321 (MIR) and 0.99 ng.m<sup>-3</sup> in Lastours (LST)). For As, the sites of LST (average value 0.27 ng.m<sup>-3</sup>) and CDS  
322 (0.30 ng.m<sup>-3</sup>) presented higher concentrations than the other sites (0.12 and 0.17 ng.m<sup>-3</sup> for CBP and  
323 MIR, respectively). Finally, the Ni concentration in LST (average value of 0.29 ng.m<sup>-3</sup>) was significantly  
324 higher than in CDS (0.19 ng.m<sup>-3</sup>), whereas CBP and MIR presented intermediate concentrations (0.26  
325 and 0.27 ng.m<sup>-3</sup>).

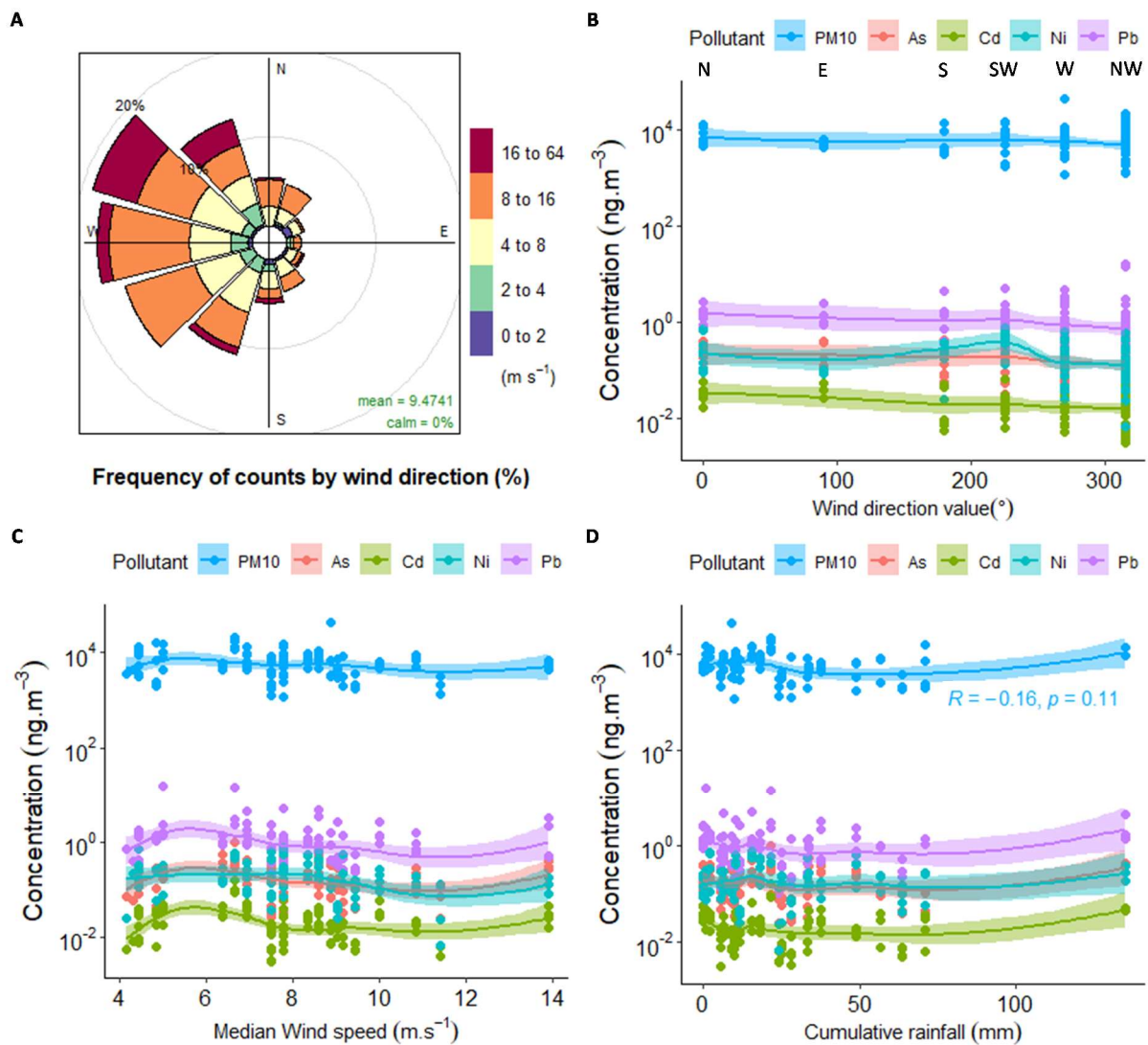
326 Concerning seasonal variations in Pb, As, Ni, and Cd mass concentrations, Ni exhibited the same trend  
327 as PM<sub>10</sub>, with higher concentrations in spring and reduced levels in autumn 2022. Pb, As, and Cd  
328 showed similar patterns: higher concentrations in winter/spring than in summer, with the lowest  
329 concentrations recorded in autumn (Figure SI 2).

330

### 331 3.1.1. Abiotic parameters' influence on PM<sub>10</sub> concentration for the different 332 sites

333 Figure 3 illustrates the behaviour of the five regulated pollutants (PM<sub>10</sub>, As, Cd, Ni and Pb) with respect  
334 to different abiotic parameters; fitted lines are included to highlight trends. During the recorded  
335 period, the most frequent and strongest winds occurred from the northwest (Figure 3 A). Regarding  
336 these abiotic parameters, PM<sub>10</sub>, As, Cd and Pb behaved similarly, but Ni showed a different trend, with  
337 increasing concentrations when the winds blew from the southwest direction, and decreasing  
338 concentrations when wind direction was from the east (Figure 3 B – zoomed figure is available in Figure

339 SI 3). Finally, a weak non-significant negative correlation was also found between PM<sub>10</sub> mass  
 340 concentration and precipitation (Figure 3 D).



341  
 342 Figure 3: Abiotic parameters: Wind rose for the recorded period at the GPS point 43°20'52" N, 2°23'29" E (A), mass  
 343 concentrations of PM<sub>10</sub>, Pb, As, Ni and Cd with respect to wind direction (B), mean wind speed (C) and cumulative  
 344 precipitation (D). In graph (B), letters represent the wind direction. In graph (D),  $R$  = the strength of the linear relationship  
 345 (Spearman correlation) and  $p$  = its statistical significance. For graphs (A, B, and C): trend lines have been added (LOESS smooth  
 346 line).

347 3.2. Tillandsia usneoides serve as biomonitors of metal(loid) composition of  
 348 the atmosphere

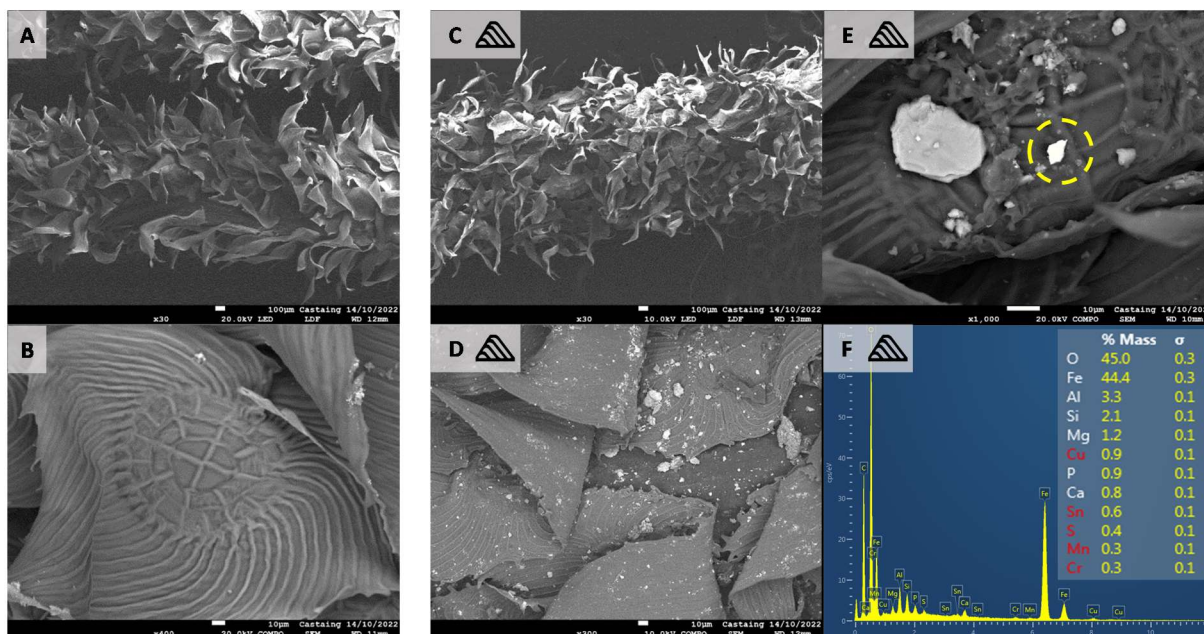
349 As previously explained, the results presented here take into account, both adsorbed and potentially  
350 absorbed fractions. This is in line with our objective of not making a distinction between what  
351 remained on the plant surface and what was taken up by the plant tissue after atmospheric deposition.

352

### 353 3.2.1. SEM-EDX observations: atmospheric deposits on unexposed and 354 exposed *T. usneoides*

355 SEM-EDX observations show the general morphology and the trichome structure in the shields of an  
356 unexposed *Tillandsia usneoides* (Figure 4-A&B). Contrastingly, the corresponding images of a plant  
357 exposed for 6 months at La Combe du Saut (CDS, Figure 4-C to F) show a homogeneous distribution of  
358 atmospheric depositions on the plant surface, with coarse particles (from 2.5  $\mu\text{m}$  to 20  $\mu\text{m}$ ) along with  
359 numerous fine particles (< 2.5  $\mu\text{m}$ ) (Figure 4-D). A majority of the EDX spectra show the presence of Si  
360 and O, indicating possible deposition of quartz ( $\text{SiO}_2$ ) (observations not shown). The spectrum shown  
361 in Figure 4-F however underlines the presence of O, Fe, Al and traces of Cu, Sn, Mn and Cr.

362



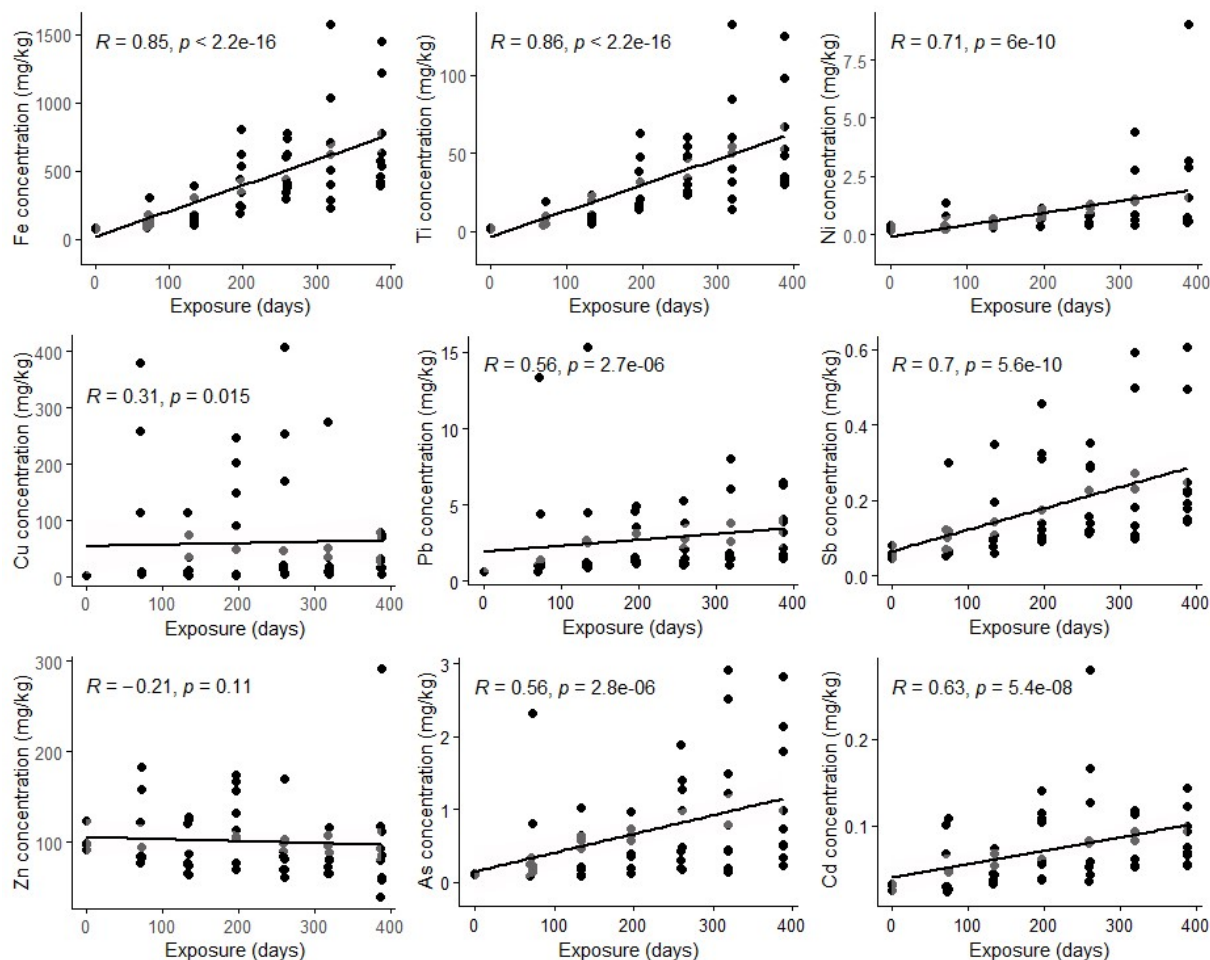
363  
 364 Figure 4: SEM-EDX observations of unexposed (left images: A and B) and *T. usneoides* exposed for 6 months (right images: C,  
 365 D, E and F) at the site of La Combe du Saut (CDS). Overview of the unexposed plant (A), and trichomes structure (B). General  
 366 observation of the exposed plant (C), Atmospheric deposits on the trichome structure (D), Atmospheric particle (surrounded  
 367 in yellow) enriched in Fe and Al (according to the EDX spectrum) observed on a trichome (E and F).

368

### 369 3.2.2. Kinetics of atmospheric deposition (and potential uptake) by *T.*

#### 370 *usneoides*.

371 For most of the elements, the kinetics of atmospheric deposition on epiphytic plants (Figure 5) showed  
 372 a linear increasing trend over a one-year period, with R values ranging from 0.56 (Pb and As) to 0.86  
 373 (Ti). On the other hand, a lower correlation between concentration and exposure time was observed  
 374 for Cu, while no clear trend could be observed for Zn.



375

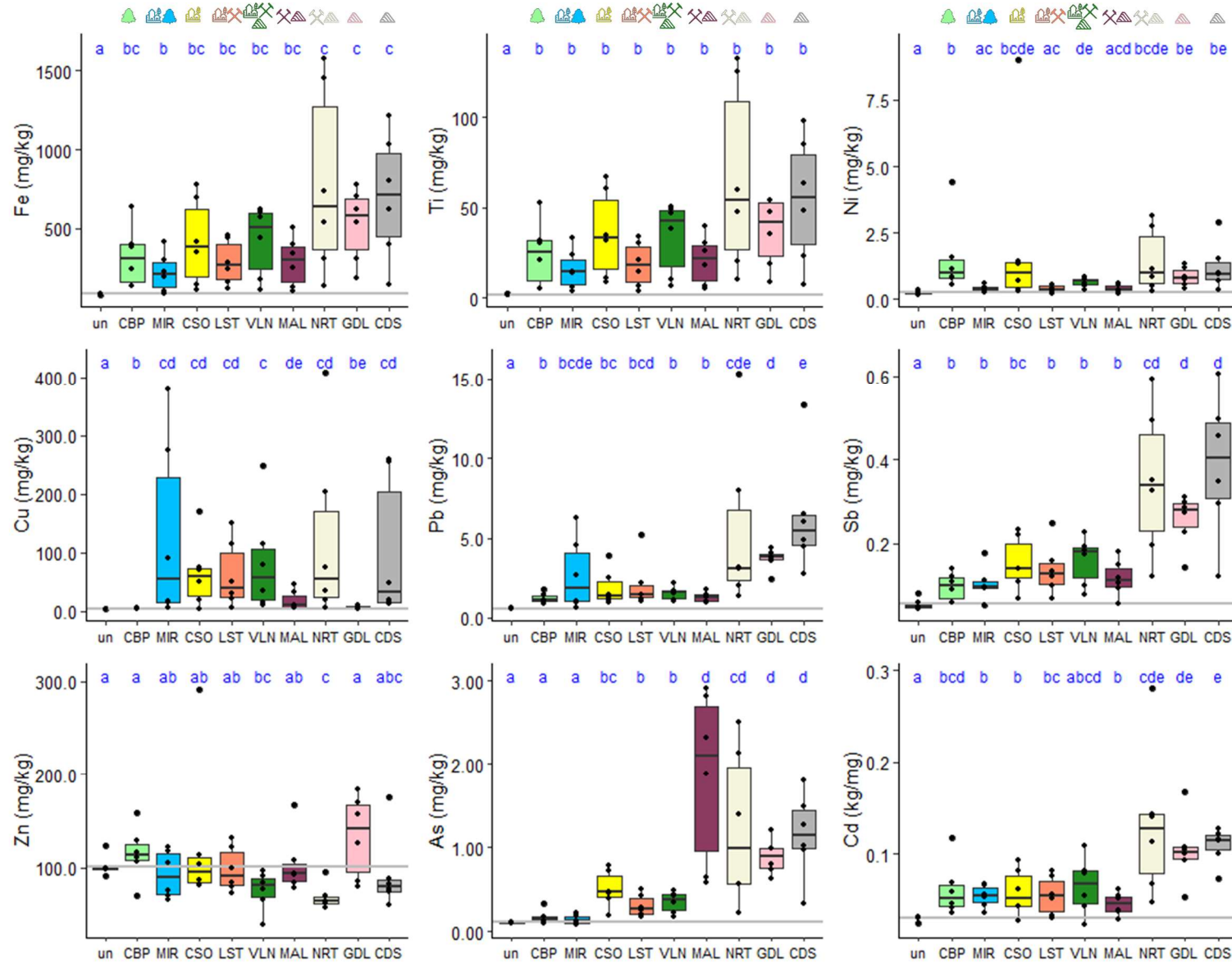
376 Figure 5: Atmospheric deposition over one year of exposure for the 9 considered elements.  $R$  = strength of the linear  
 377 relationship (Spearman) and  $p$ = its statistical significance.

378

### 379 3.2.3. Effect of the location on elemental composition of *T. usneoides*

380 Figure 6 shows the metal(loid) concentrations in *T. usneoides* in the 9 investigated locations for the 9  
 381 target elements, without any discrimination of the exposure time. Data on all other elements can be  
 382 found in the supporting information (Table SI 5). Significant differences are found between sites for  
 383 As, Pb, Sb and Cd (Figure 6). A net distinction between sites can be made for As: the highest levels of  
 384 this metalloid were found in MAL (Malabau), NRT (Nartau), GDL (Gué de Lassac) and CDS (La Combe  
 385 du Saut), followed by CSO (Conques sur Orbiel), Lastours (LST) and Villanière (VLN). The lowest As  
 386 concentrations were observed in plants positioned in MIR (Miraval) and Gouffre de Cabrespine (CBP),

387 which were at the same level as the unexposed (control) plants. For Pb, NRT and CDS sites but also  
388 GDL, MIR and LST sites to a lesser extent, exhibited the highest concentrations in *T. usneoides*. For Sb  
389 and Cd, the sites of Nartau (NRT), Gué de Lassac (GDL), and La Combe du Saut (CDS) presented higher  
390 concentrations than the other sites.

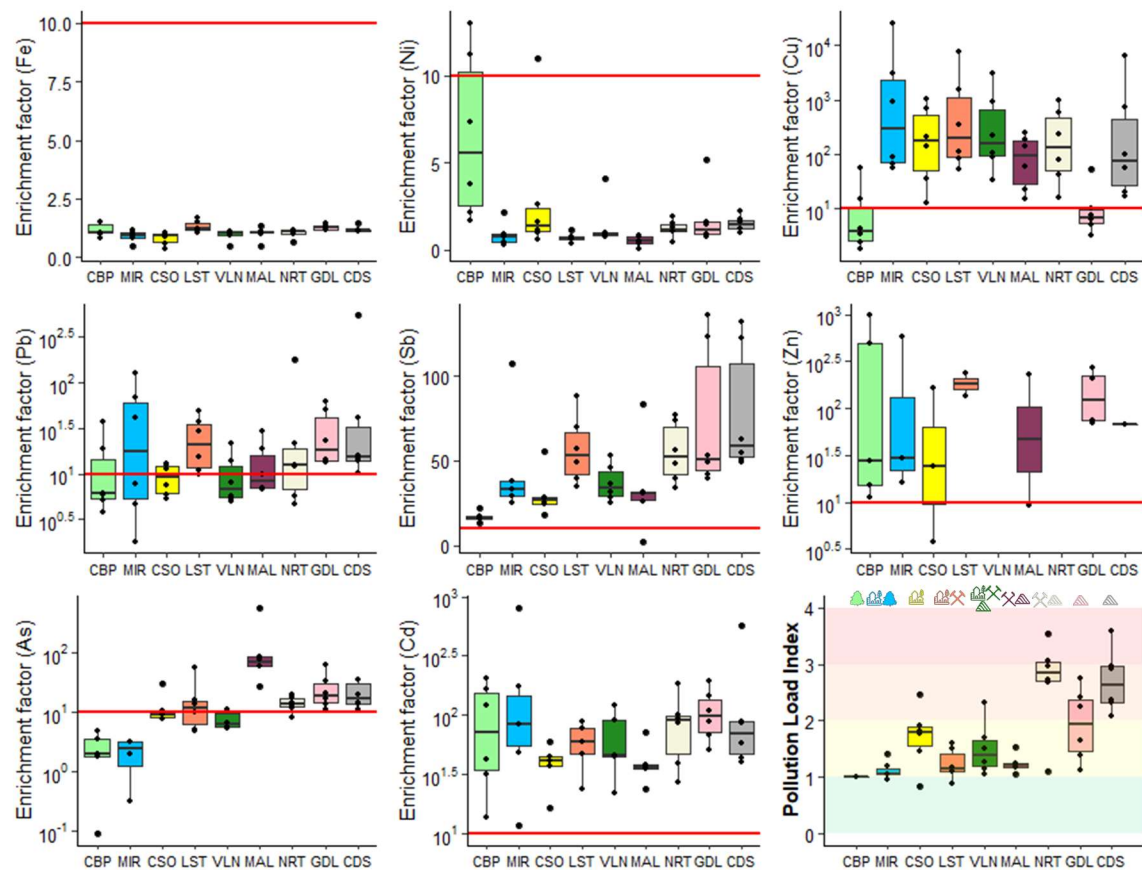


391

392 Figure 6: Elemental concentrations of Fe, Ti, Ni, Cu, Pb, Sb, Zn, As, and Cd ( $\text{mg.kg}^{-1}$ ) in *T. usneoides* at the 9 studied sites from the Orbiel valley. un = unexposed plants; CBP = Gouffre de  
 393 Cabrespine; MIR = Miraval; CSO = Conques sur Orbiel; LST= Lastours; VLN = Villanière; MAL = Malabau; NRT = Nartau; GDL = Gué de Lassac; CDS = La Combe du Saut. Horizontal dotted line =  
 394 mean for unexposed plants. Blue letters represent the statistical difference between sites (non-parametric Mann-Whitney tests).

395        3.2.4. Evaluation of contamination levels and determination of atmospheric  
396 sources

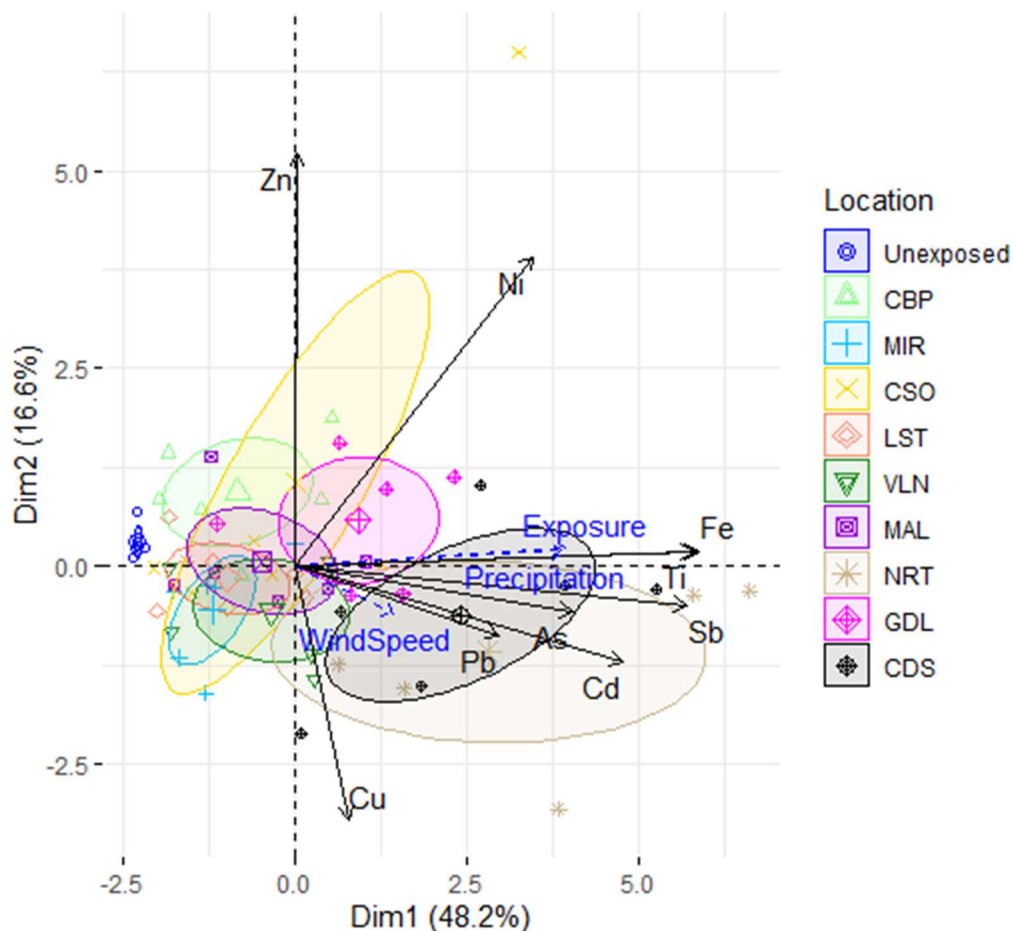
397 Results of EF are reported in Figure 7. No significant enrichment in Fe and Ni ( $EF \ll 10$ ) is indicated for  
398 the different studied locations, whereas enrichment in Cd, Sb and Zn is observed in all sites (except for  
399 VLN and NRT – no data). With the exception of CBP and GDL, all the locations present an enrichment  
400 in Cu. An enrichment in Pb is also observed for *T. usneoides* placed in the sites of MIR, LST, NRT, GDL  
401 and CDS (median EF values greater than 10). Finally, an enrichment in As is also observed in the plants  
402 exposed in MAL, NRT, GDL, and in LST sites to a lesser extent (median EF values greater than 10; see  
403 Figure 7).



404

405 Figure 7: Indicators (EF and PLI) for environmental status assessment of the 9 studied sites of the Orbiel valley : CBP= Gouffre de Cabrespine; MIR= Miraval; CSO= Conques sur Orbiel; LST=  
 406 Lastours; VLN= Villanière; MAL= Malabau; NRT= Nartau; GDL= Gué de Lassic; CDS= La Combe du Saut. **Enrichment factors (EF)** calculated **using crustal composition** (Rudnick and Gao, 2003) of  
 407 the 8 elements of interest (except Ti) in *T. usneoides*. Please note that a log scale is used except for Fe and Ni. The red line represents the threshold value EF = 10. The **Pollution Load Index (PLI)**  
 408 was calculated from *T. usneoides* data and from the concentrations of the 9 elements studied. *PLI < 1 in green (no pollution), 1 = PLI < 2 in yellow (mild pollution), 2 = PLI < 3, in orange (moderate*  
 409 *pollution), PLI ≥ 3 in red (severe pollution).*

410 The PCA results are reported in Figure 8, which highlight that 64.8 % of the variance contained in the  
 411 data are retained by the first 2 principal components (PCs).



412  
 413 Figure 8: **PCA data results** for *T. usneoides*: biplot of individuals (samples) and variables (elements and abiotic parameters).  
 414 CBP = Gouffre de Cabrespine; MIR = Miraval; CSO = Conques sur Orbiel; LST= Lastours; VLN = Villanière; MAL = Malabau; NRT  
 415 = Nartau; GDL = Gué de Lassac; CDS = La Combe du Saut. *Note that the values of the axes represent the coordinates of*  
 416 *individuals, not the variance.*

417 As shown in Figure SI 4, Fe, Ti, Sb, Zn, Ni and Cd emerge as the primary contributors to the PCs.  
 418 Positively correlated variables include Fe, Ti, Sb, Cd and As, with Ni and Pb to a lesser extent.  
 419 Additionally, negatively correlated variables (Zn and Cu) are observed in the orthogonal dimension.  
 420 Thus, 3 groups of individuals are observed on the PC1 axe: (i) unexposed plants presenting low values  
 421 for the 9 elements considered here; (ii) NRT and CDS locations displaying high values in Fe, Ti, Sb, Cd,  
 422 As and Pb; and (iii) an intermediary group composed of the 7 other locations (CBP, CSO, GDL, LST, MAL,  
 423 MIR, VLN).

### 424 3.2.5. Assessment of the environmental status with pollution index

425 The results of PLI calculations, performed while comparing the concentrations measured in plants from  
426 the control site of CBP, are shown in Figure 7 (bottom right). A mild pollution index is found for CBP,  
427 MIR, LST, MAL and GDL (median values: 1 =  $PLI < 2$ ) whereas a moderate pollution index is obtained for  
428 NRT and CDS (median values: 2 =  $PLI < 3$ ).

429

## 430 4. Discussion

### 431 4.1. Global air quality in the Orbiel valley

#### 432 4.1.1. Assessment through $PM_{10}$ atmospheric concentrations

433 The values of  $PM_{10}$  mass concentration and elemental composition measured in the present study are  
434 in accordance with previously reported data for the same area as described in two technical reports  
435 from the French geological survey (BRGM) in 2006 and 2020 (Bausch and Merlen, 2021; Durif et al.,  
436 2006).

437 The present results (obtained in 2022) in the Orbiel valley have also been compared to similar data on  
438 other sites in France and worldwide. Two French rural sites with and without industrial background  
439 have been used for comparison: the site of Peyrusse-Veille for the period of 2022, and the former  
440 metallurgical plant of Viviez for the period of 2021 ([www.atmo-occitanie.org](http://www.atmo-occitanie.org)). In addition, two foreign  
441 rural sites with a mining history have also been considered for the comparison: the Nerva village site  
442 near the former Rio Tinto mine in Spain for the period of March 2009 – March 2010 (Sánchez de la  
443 Campa et al., 2011) and the Pitcher site near the “Chat” tailings of a former mine in the USA for the  
444 period of July 2005 – September 2006 (Zota et al., 2009). Overall, with a few exceptions, results for air  
445 quality in the Orbiel valley were better than those obtained in the 4 sites chosen for comparison. When  
446 comparing the French rural sites, we find that investigated locations in the Orbiel valley show lower  
447 concentrations of  $PM_{10}$ , Cd and Ni, than the other 2 French sites; for  $PM_{10}$ , the average values were 11

448  $\mu\text{g}\cdot\text{m}^{-3}$  in both Peyrusse-Vielle and Viviez. For Cd, and Ni, the corresponding values were 0.04 and 1  
449  $\text{ng}\cdot\text{m}^{-3}$  and 0.45 and 0.40  $\text{ng}\cdot\text{m}^{-3}$  in Peyrusse Vielle and Viviez, respectively. The concentrations of As  
450 were locally higher in the Orbiel valley (in CDS and LST) than in Peyrusse-Vielle (0.19  $\text{ng}\cdot\text{m}^{-3}$ ), but lower  
451 than that recorded at the Viviez site (0.40  $\text{ng}\cdot\text{m}^{-3}$ ). Similarly, Pb concentrations were locally higher in  
452 the Orbiel valley (in CDS and MIR) than in Peyrusse-Vielle (1.3  $\text{ng}\cdot\text{m}^{-3}$ ), but lower or in the same range  
453 as that recorded at the Viviez site (2.7  $\text{ng}\cdot\text{m}^{-3}$ ). Overall, the concentrations ( $\text{PM}_{10}$ , Pb, As, Cd and Ni) in  
454 the former mining sites in Spain and in the USA were higher than in the Orbiel valley, with the exception  
455 of the Pitcher site where As values were < LOD, and undetermined for Cd and Ni.

456

#### 457 4.1.2. Assessment through biomonitoring using *Tillandsia usneoides*

458 The metalloid concentrations in unwashed plants following exposure for 2 months in the Orbiel valley,  
459 were compared with those on unwashed plants exposed for 36 days in a rural site near Pisa in Italy  
460 (Pellegrini et al., 2014; rural/remote (RR) site), and with unwashed plants exposed for 8 weeks in two  
461 traffic sites in the city of São Paulo in Brazil (Figueiredo et al., 2007; Cerqueira César (CC) and  
462 Congonhas (CG) sites). This comparison allowed to assess the total atmospheric deposition depending  
463 on the exposure site. Overall, among the eight elements compared, the concentrations of Ni, Cd, Fe  
464 and Sb in the plants exposed in the Orbiel valley (average concentrations excluding the CBP site) were  
465 lower than the corresponding values observed in plants exposed in a rural area in Italy ( $\sim 8, 3, 2$  and 2  
466 times, respectively), or sites under dense traffic in the city of São Paulo (about 6 times for Fe and 7  
467 times for Sb) (Table SI 6). It is worth noting that the values for Fe and Sb were higher at the GDL site  
468 than at the rural site in Italy. With respect to the other 4 elements, the average concentration of Zn in  
469 the Orbiel valley was in the same range as that in the rural site in Italy (around 100  $\text{mg}\cdot\text{kg}^{-1}$ ) and was  
470 1.6 times higher than in the traffic-ridden sites of São Paulo. Significantly, the average concentration  
471 of Cu in the Orbiel valley after two months of exposure was 14 times higher than in the Italian site (no  
472 data for São Paulo). Finally, for As and Pb, the average concentrations in the Orbiel valley were 2 times

473 higher than in the studied site in Italy (for both elements) and in the traffic-ridden sites in São Paulo  
474 (1.4 times for As, no data for Pb in São Paulo) (Table SI 6).

475 Thus, although the Orbiel valley is home to a large number of mining sites, the resuspension of PM and  
476 its deposition on *T. usneoides* appears to be limited.

477

## 478 4.2. Identification of potential sources of metal(loid) in the atmosphere

### 479 4.2.1. Source apportionment using abiotic parameters and PM<sub>10</sub> trends

480 The concentrations of As, Cd, and Pb show similar behaviour with respect to wind direction, the median  
481 wind speed and the cumulative rainfall, as well as the observed similarity in seasonal trend. This  
482 strongly indicates that that these elements come from the same source and from similar atmospheric  
483 processes (Figures 2 and 3). In their study on the influence of Saharan mineral dust on PM<sub>10</sub>  
484 concentration and composition in the city of Constantine (Algeria), Lokorai et al. (2021) reported that  
485 a similarity in temporal evolution of the elements could indicate a common origin. In contrast, the  
486 different seasonal behaviour of Ni and above all, its different behaviour in relation to the wind  
487 direction, suggest that its source should be different from that of As, Cd and Pb (Figures SI 2 and SI 3).  
488 The influence of the surface temperature was not examined further in view of the low concentrations  
489 measured during summer 2022. Lastly, the frequent and strongest winds occurring from the  
490 west/northwest direction were associated with air masses carrying rainfall (Figure SI 5). In fact, during  
491 the sampling period, the valley experienced one extreme precipitation event (cumulated rain >100  
492 mm) linked to southwardly winds, or “Cévenol event” (Figure SI 5). Our data indicate that this event  
493 was also associated with a slight increase in atmospheric concentrations for PM<sub>10</sub>, As, Pb, Ni and Cd  
494 (Figure 3 D), but the overall precipitation data through one complete year, shows (Figure 3 D, R= –  
495 0.16) a small decreasing trend for PM<sub>10</sub> washout, suggesting that washout during rainfall was certainly  
496 quite low. Thus, in this case, dry deposition by sedimentation seems to be the most efficient process  
497 for coarse particles deposition (Grantz et al. 2003).

498

499 **4.2.2. Atmospheric biomonitoring brings new insights to sources' tracing**

500 The elemental composition of *T. usneoides* (Figure 6 and Table SI 5) allowed to identify the most  
501 exposed sites in the Orbiel valley and also to successfully identify the potential sources of air  
502 contamination in this valley. As already pointed out (section 4.1.2), the plants exposed in NRT, GDL and  
503 CDS sites had higher concentrations of Pb, Sb, As and Cd than those in the other places. The plants that  
504 were exposed close to the MAL site also had high levels of As. These 4 biomonitored sites were located  
505 near 4 of the 5 waste storages studied here.

506 Moreover, results of EF calculation for epiphytic plants (Figure 7) indicate that Ni and Fe (EF values <<  
507 10) were the non-enriched elements in this valley with a local rock and soil dust origin. On the other  
508 hand, the enriched elements in the valley (median EF values  $\geq 10$ ) were Cu, Zn, Sb and Cd, but also As  
509 and Pb for some sites. As reported in Figure 7, the MIR site shows an enrichment in Pb, while the MAL  
510 site presents the highest enrichment in As. Both elements appear as enriched in LST, as well as in NRT,  
511 GDL and CDS sites. We remind here that the sites of MAL, NRT, GDL and CDS were considered as the  
512 most exposed to mining activities in this valley including waste storage, old mining extractions and  
513 industries. This observation thus indicates inputs from sources other than the natural local rocks and  
514 soil dust, pointing to potential anthropogenic origins. However, in the Orbiel valley, there is a  
515 considerable natural enrichment of elements such as As in the geological bedrock, which provides a  
516 rationale for the intense extractive activities that occurred for centuries in this area. Therefore, instead  
517 of the average upper crust values, we used for comparison, the average local pedo-geochemical  
518 background (PGB) concentrations of the various metal(loid)s recently determined by Delplace and al.  
519 (2020) to recalculate the EF values. Results (Figure SI 6) illustrate that lower EF values were obtained,  
520 especially for As and Pb, indicating that in this area, the As and Pb content could be associated with  
521 resuspension of soil dusts due to local wind erosion. With regard to the enrichment in Pb in the MIR  
522 area (upstream part of the Orbiel river), it should be noted that Heydon et al. (2023) also identified the

523 highest Pb concentrations in the Orbiel river within this area. These results could be an indication that  
524 several ecosystems in this part of the valley could be contaminated with Pb.

525 To further link our results to potential sources, a PCA was performed (Figure 8). The 1<sup>st</sup> component  
526 accounted for 48.2% of the variance with a co-variance observed among several elements: Fe (10.3%  
527 of the total variance), Ti (10.1%), Sb (9.7%), Cd (6.8%), As (4.9%), and to a lesser extent, Ni and Pb  
528 (respectively, 3.6%, 2.6%) (see Figure SI 4 for more details). As an explanation, Fe, Ti and Ni were  
529 supposed to be associated to natural local rock and soil dust sources (as suggested by the EF values).

530 On the other hand, Sb, Cd and As (and Pb), with EF values > 10, were supposed to be associated to  
531 possible anthropogenic sources. Finally, enrichment factors associated with the co-variation observed  
532 for the different elements indicate possible impact of dust and resuspension of anthropogenic  
533 materials sources (road, waste storage). To confirm this hypothesis, a PCA was done with PM<sub>10</sub> data  
534 collected for the 4 monitored sites (Figure SI 7): 72.1% of the variance was retained in the first  
535 component (82.5 % for the first 2 components). The co-variation of all the elements, with the variables  
536 explaining from 9.1% (Zn) to 6.4% (Pb) of the variance, confirmed our previous finding from results on  
537 *T. usneoides*, that resuspensions of both dust and materials of anthropogenic origin, are the main  
538 sources of atmospheric contamination in the valley.

539

### 540 4.3. Assessment of the environmental status of the Orbiel valley

#### 541 4.3.1. Indicators to assess the environmental status

542 Pollution load indexes calculated in epiphytic plants indicated a moderate contamination for NRT and  
543 CDS sites, and a mild pollution for the other locations (Figure 7). These PLI values are higher than those  
544 reported by Chen et al. (2022), who used pine needle as bioindicators of air quality and found none to  
545 mild pollution in different sites in Wuhan and Yichang. However, we note here that, different  
546 bioindicators and elements were selected in the two studies for the PLI calculations. In our case, PLI  
547 results are in accordance with our previous results, i.e., a moderate contamination was detected in the

548 valley using conventional instrumentation ( $PM_{10}$  results in accordance to EU standards) and  
549 biomonitoring technique (low concentrations after 2 months of exposure when compared with values  
550 reported in the literature), and the NRT and CDS sites (PLI and PCA results) were found to be the most  
551 contaminated sites in the valley. Calculation of PLI has allowed to summarize this information, classify  
552 the sites with respect to each other, and provided a simple way to assess the environment status of  
553 the area.

554

#### 555 4.3.2. Using biomonitoring to better estimate chronic exposure

556 The kinetics of atmospheric fallouts on *Tillandsia* species have been reported in a few recent studies,  
557 but the conclusions drawn have not been unanimous. Parente et al. (2023), assessed the air quality of  
558 residential areas in the vicinity of the Brumadinho collapsed tailings dam in Brazil. They observed  
559 higher concentrations of As, Ni and Hg in *T. usneoides* after 15 days than after 45 days of exposure,  
560 suggesting a non-linear accumulation behaviour for these elements. However, a linear behaviour was  
561 observed for Cr, Cu, Fe and Mn. Figueiredo et al. (2007) studied the urban area of São Paulo in Brazil,  
562 and Martínez-Carrillo et al. (2010), in their investigation on the Tula–Tepeji industrial area in Central  
563 Mexico, reported a maximal accumulation in *T. usneoides* after about 2 months of exposure. Isaac-  
564 Olivé et al. (2012), also showed for the Tula–Tepeji industrial area (Central Mexico) that the  
565 concentration of lanthanide elements reached a maximum after 10 weeks. Schreck et al. (2016), using  
566 *Tillandsia capillaris* (in the mining district of Oruro, Bolivia), reported an almost linear response for As,  
567 Cd, Hg, and Sn, but not for Ag, Pb, Sb, and Zn after 5 months of exposure. Finally, Schreck et al. (2020),  
568 in their study on the old mining district of Cartagena-La Unión in Spain, observed a global increase in  
569 Zn, Pb, As and Cd over time (12 months – *T. usneoides*).

570 In our study, we observe “strong” ( $R > 0.5$ ) linear deposition up to 12 months of exposure for Fe, Ti, Ni,  
571 Sb, Cd, Pb and As (Figure 5). This suggests that this plant species could be efficiently used under these  
572 conditions of a former mining district and allows continuous monitoring of these elements over at least

573 one year. However, for Zn and Cu, such conclusions could not be made; these elements can be  
574 identified as nutrients. Moreover, it is interesting to mention that Martínez-Carrillo et al. (2010)  
575 observed low accumulation rates for elements such as Cu, Zn (and Fe) in *T. usneoides*, when comparing  
576 them to those on filters. Regarding Cu and Zn, results of our two PCAs did not converge, confirming  
577 our previous finding, that these micro-nutrients show a different response (non-linear deposition)  
578 when biomonitoring with *T. usneoides*. The kinetics of atmospheric deposition on *Tillandsia* species  
579 over one year of exposure and with frequent inter-sampling periods have not been discussed in detail  
580 in these other studies (Figueiredo et al., 2007; Isaac-Olivé et al., 2012; Martínez-Carrillo et al., 2010;  
581 Parente et al., 2023; Schreck et al., 2016; Schreck et al., 2020). One plausible explanation for the  
582 variation in Cu and Zn behavior in *T. usneoides* could be the physicochemical properties of Cu- and Zn-  
583 bearing mineral particles (size, speciation and solubility) which might have led to their preferential  
584 leaching. The second explanation concerns physiological processes, i.e. differential uptake according  
585 to requirements or excretion/detoxification processes involving these elements (Schreck et al., 2016).  
586 In our study, dilution attributed to plant growth has been ruled out, as we do not see this effect on  
587 other elements. There is the case of Fe, a micro-nutrient, which presented a linear kinetics of  
588 deposition onto plants. We attribute this result to the presence of Fe (hydr)oxides (as indicated by  
589 SEM-EDX analyses, Figure 4) and the low solubility and bioavailability of these (hydr)oxides.

590

591 Despite 2022 being recorded as an unusual year with respect to climate with extreme climatic values  
592 and low precipitation, these epiphytic plants appear to be efficient indicators to follow air quality in  
593 the Orbiel valley. Moreover, due to climate change and global warming, extreme meteorological  
594 parameters will tend to be more generalised in our latitudes. This is particularly relevant since, as  
595 reported by Mandal et al. (2023), climate change can influence PM distribution and increase total PM<sub>2.5</sub>  
596 content in the atmosphere due to their longer lifetime, especially in summer.

597 Finally, in terms of chronic exposure and potential health risks through inhalation, it is worth citing  
598 WHO reports that mention that fine particle pollution has health impacts even at very low

599 concentrations, and there is no threshold below which no damage to health is observed (World Health  
600 Organization, 2016). Our relatively simple, cheap and convenient approach could therefore be  
601 generalised to understand chronic exposure to metal(loid) rich particles. Nevertheless, more research  
602 is needed to extend biomonitoring to the other PM constituents (PAH, for example).

603

## 604 5. Conclusion

605 In 2022, the air quality in the Orbiel valley was found to be good, with PM<sub>10</sub> levels in line with the EU  
606 standards and in accordance with the two technical reports issued by the French geological survey  
607 (BRGM) for the same area in 2006 and 2020. Moreover, the concentrations of detected elements in  
608 the exposed plants were globally lower than the concentrations on *T. usneoides* reported in the  
609 literature. Our different results, such as the influence of the abiotic parameters on PM<sub>10</sub>  
610 concentrations, PCAs results done on PM<sub>10</sub> and *T. usneoides* data, as well as EF calculated in *T.*  
611 *usneoides*, suggest that resuspensions of dust and of anthropogenic materials could be the sources of  
612 most of the studied elements. Finally, the calculation of pollution indexes made it possible to  
613 summarise the information, to classify the sites, and to identify Nartau and La Combe du Saut sites  
614 (situated in waste storage and former mining industry area), as the most affected.

615 To fully understand the human exposure routes in the valley, more work is needed that involves i)  
616 measuring the PM oxidative potential (OP) for the inhalation route, and ii) determining toxic elements  
617 linked to atmospheric deposition in vegetables for the food route to assess the risks linked to these  
618 deposits on food. An epidemiological study would also help to further understand the association  
619 between different exposure routes and the potential health risks to the inhabitants.

## 620 Acknowledgments

621 This work was carried out under the framework of the “DiagnOSE” project, funded in part by the Region  
622 Occitanie Pyrénées – Méditerranée, France, and managed by INP Toulouse. This work was also  
623 supported by the CNRS INSU EC2CO program, through the PhytAsOrb project. Aude Calas (first author)  
624 was financially supported for 2 years by the DiagnOSE project. We thank Manuel Henry for his technical  
625 help in acidic mineralisation in the clean laboratory; Rémi Freydier and Léa Causse from the AETE-ISO  
626 Plateform of OSU OREME, at the University of Montpellier, and Camille Duquenoy from the Service  
627 ICP-MS at the Midi-Pyrénées Observatory of Toulouse, for their assistance with ICP-MS analyses. We  
628 also express our gratitude to our colleague Stéphane Le Blond du Plouy from the Centre de Micro  
629 Caractérisation Raimond Castaing in Toulouse for his technical support in SEM-EDX analysis of *T.*  
630 *usneoides* and Dr. Revathi Bacsa for editorial assistance. Finally, this study could not have been  
631 conducted without the precious help and technical support for our atmosphere experiments from the  
632 local population, and especially Gilles Marty.

633 **References**

- 634 Bausch, P., Merlen, R., 2021. Etude des poussières atmosphériques dans le district minier de la vallée de l'Orbiel  
635 (11). Rapp. d'étude EVADIES - BRGM 1–147.
- 636 Blondet, I., Schreck, E., Viers, J., Casas, S., Jubany, I., Bahí, N., Zouiten, C., Dufrécho, G., Freydier, R., Galy-Lacaux,  
637 C., Martínez-Martínez, S., Faz, A., Soriano-Disla, M., Acosta, J.A., Darrozes, J., 2019. Atmospheric dust  
638 characterisation in the mining district of Cartagena-La Unión, Spain: Air quality and health risks assessment.  
639 *Sci. Total Environ.* 693. <https://doi.org/10.1016/j.scitotenv.2019.07.302>
- 640 Bondu, R., Casiot, C., Pistre, S., Batiot-Guilhe, C., 2023. Impact of past mining activities on water quality in a karst  
641 area in the Cévennes region, Southern France. *Sci. Total Environ.* 873.  
642 <https://doi.org/10.1016/j.scitotenv.2023.162274>
- 643 Chen, M., Lu, W., Hou, Z., Zhang, Y., Jiang, X., Wu, J., 2017. Heavy metal pollution in soil associated with a large-  
644 scale cyanidation gold mining region in southeast of Jilin, China. *Environ. Sci. Pollut. Res.* 24, 3084–3096.  
645 <https://doi.org/10.1007/s11356-016-7968-3>
- 646 Chen, Y., Ning, Y., Bi, X., Liu, J., Yang, S., Liu, Z., Huang, W., 2022. Pine needles as urban atmospheric pollution  
647 indicators: Heavy metal concentrations and Pb isotopic source identification. *Chemosphere* 296, 134043.  
648 <https://doi.org/10.1016/j.chemosphere.2022.134043>
- 649 Csavina, J., Field, J., Taylor, M.P., Gao, S., Landázuri, A., Betterton, E.A., Sáez, A.E., 2012. A review on the  
650 importance of metals and metalloids in atmospheric dust and aerosol from mining operations. *Sci. Total*  
651 *Environ.* 433, 58–73. <https://doi.org/10.1016/j.scitotenv.2012.06.013>
- 652 Dasch, J.M., Wolff, G.T., 1989. Trace inorganic species in precipitation and their potential use in source  
653 apportionment studies. *Water, Air, Soil Pollut.* 43, 401–412. <https://doi.org/10.1007/BF00279205>
- 654 de Fleury, M., Kergoat, L., Grippa, M., 2023. Hydrological regime of Sahelian small waterbodies from combined  
655 Sentinel-2 MSI and Sentinel-3 Synthetic Aperture Radar Altimeter data. *Hydrol. Earth Syst. Sci.* 27, 2189–  
656 2204. <https://doi.org/10.5194/hess-27-2189-2023>
- 657 Delplace, G., Viers, J., Schreck, E., Oliva, P., Behra, P., 2022. Pedo-geochemical background and sediment  
658 contamination of metal(loid)s in the old mining-district of Salsigne (Orbiel valley, France). *Chemosphere*

- 659 287. <https://doi.org/10.1016/j.chemosphere.2021.132111>
- 660 Desaulty, A., Négrel, P., Kloppmann, W., Petelet-Giraud, E., Gaboriau, H., 2016. Diagnostic multi-isotopique sur  
661 le site de La Combe du Saut (district de Salsigne - Aude). Rapp. Final BRGM/RP-65, p.69.
- 662 Drouhot, S., Raoul, F., Crini, N., Tougard, C., Prudent, A.S., Druart, C., Rieffel, D., Lambert, J.C., Tête, N., Giraudoux,  
663 P., Scheifler, R., 2014. Responses of wild small mammals to arsenic pollution at a partially remediated  
664 mining site in Southern France. *Sci. Total Environ.* 470–471, 1012–1022.  
665 <https://doi.org/10.1016/j.scitotenv.2013.10.053>
- 666 Durif, M., Fable, S., Gay, G., Karoski, N., Meunier, L., Tack, K., 2006. Evaluation quantitative des risques sanitaires  
667 liés à l' inhalation des particules métalliques issues des sols de surface par les populations riveraines du  
668 site d' exploitation minier du site. Rapp. d' étude Ineris 26.
- 669 Elbaz-Poulichet, F., Resongles, E., Bancon-Montigny, C., Delpoux, S., Freydier, R., Casiot, C., 2017. The  
670 environmental legacy of historic Pb-Zn-Ag-Au mining in river basins of the southern edge of the Massif  
671 Central (France). *Environ. Sci. Pollut. Res.* 24, 20725–20735. <https://doi.org/10.1007/s11356-017-9669-y>
- 672 Esmailirad, S., Lai, A., Abbaszade, G., Schnelle-Kreis, J., Zimmermann, R., Uzu, G., Daellenbach, K., Canonaco, F.,  
673 Hassankhany, H., Arhami, M., Baltensperger, U., Prévôt, A.S.H., Schauer, J.J., Jaffrezo, J.L., Hosseini, V., El  
674 Haddad, I., 2020. Source apportionment of fine particulate matter in a Middle Eastern Metropolis, Tehran-  
675 Iran, using PMF with organic and inorganic markers. *Sci. Total Environ.* 705, 135330.  
676 <https://doi.org/10.1016/j.scitotenv.2019.135330>
- 677 Figueiredo, A.M.G., Nogueira, C.A., Saiki, M., Milian, F.M., Domingos, M., 2007. Assessment of atmospheric  
678 metallic pollution in the metropolitan region of São Paulo, Brazil, employing *Tillandsia usneoides* L. as  
679 biomonitor. *Environ. Pollut.* 145, 279–292. <https://doi.org/10.1016/j.envpol.2006.03.010>
- 680 Freydier, R., Viers, J., 2003. Isotopic study of lead transfer at the interface soil-plants-atmosphere. *Geophys. Res.*  
681 *Lett.* 30, 1–4. <https://doi.org/10.1029/2002GL016145>
- 682 Gerdol, R., Bragazza, L., Marchesini, R., Alber, R., Bonetti, L., Lorenzoni, G., Achilli, M., Buffoni, A., De Marco, N.,  
683 Franchi, M., Pison, S., Giaquinta, S., Palmieri, F., Spezzano, P., 2000. Monitoring of heavy metal deposition  
684 in Northern Italy by moss analysis. *Environ. Pollut.* 108, 201–208. [https://doi.org/10.1016/S0269-](https://doi.org/10.1016/S0269-7491(99)00189-X)  
685 [7491\(99\)00189-X](https://doi.org/10.1016/S0269-7491(99)00189-X)

- 686 Grantz, D.A., Garner, J.H.B., Johnson, D.W., 2003. Ecological effects of particulate matter. *Environ. Int.* 29, 213–  
687 239. [https://doi.org/10.1016/S0160-4120\(02\)00181-2](https://doi.org/10.1016/S0160-4120(02)00181-2)
- 688 Heydon, M., Perez Serrano, L., Schreck, E., Causserand, C., Pokrovsky, O.S., Behra, P., Viers, J., 2023. Role of  
689 colloids in the transfer and dispersion of trace elements into river waters through a former mining district.  
690 *Appl. Geochemistry* 155, 105736. <https://doi.org/10.1016/j.apgeochem.2023.105736>
- 691 Huertas, J.I., Huertas, M.E., Izquierdo, S., González, E.D., 2012. Air quality impact assessment of multiple open  
692 pit coal mines in northern Colombia. *J. Environ. Manage.* 93, 121–129.  
693 <https://doi.org/10.1016/j.jenvman.2011.08.007>
- 694 Isaac-Olivé, K., Solís, C., Martínez-Carrillo, M.A., Andrade, E., López, C., Longoria, L.C., Lucho-Constantino, C.A.,  
695 Beltrán-Hernández, R.I., 2012. Tillandsia usneoides L, a biomonitor in the determination of Ce, La and Sm  
696 by neutron activation analysis in an industrial corridor in Central Mexico. *Appl. Radiat. Isot.* 70, 589–594.  
697 <https://doi.org/10.1016/j.apradiso.2012.01.007>
- 698 Khaska, M., Le Gal La Salle, C., Verdoux, P., Boutin, R., 2015. Tracking natural and anthropogenic origins of  
699 dissolved arsenic during surface and groundwater interaction in a post-closure mining context: Isotopic  
700 constraints. *J. Contam. Hydrol.* 177–178, 122–135. <https://doi.org/10.1016/j.jconhyd.2015.03.008>
- 701 Lokorai, K., Ali-Khodja, H., Khardi, S., Bencharif-Madani, F., Naidja, L., Bouziane, M., 2021. Influence of mineral  
702 dust on the concentration and composition of PM10 in the city of Constantine. *Aeolian Res.* 50, 100677.  
703 <https://doi.org/10.1016/j.aeolia.2021.100677>
- 704 Mandal, M., Das, S., Roy, A., Rakwal, R., Jones, O.A.H., Popek, R., Agrawal, G.K., Sarkar, A., 2023. Interactive  
705 relations between plants, the phyllosphere microbial community, and particulate matter pollution. *Sci.*  
706 *Total Environ.* 890, 164352. <https://doi.org/10.1016/j.scitotenv.2023.164352>
- 707 Martínez-Carrillo, M.A., Solís, C., Andrade, E., Isaac-Olivé, K., Rocha, M., Murillo, G., Beltrán-Hernández, R.I.,  
708 Lucho-Constantino, C.A., 2010. PIXE analysis of Tillandsia usneoides for air pollution studies at an industrial  
709 zone in Central Mexico. *Microchem. J.* 96, 386–390. <https://doi.org/10.1016/j.microc.2010.06.014>
- 710 Parente, C.E.T., Carvalho, G.O., Lino, A.S., Sabagh, L.T., Azeredo, A., Freitas, D.F.S., Ramos, V.S., Teixeira, C., Meire,  
711 R.O., Ferreira Filho, V.J.M., Malm, O., 2023. First assessment of atmospheric pollution by trace elements  
712 and particulate matter after a severe collapse of a tailings dam, Minas Gerais, Brazil: An insight into

- 713 biomonitoring with *Tillandsia usneoides* and a public health dataset. *Environ. Res.* 233.  
714 <https://doi.org/10.1016/j.envres.2023.116435>
- 715 Pellegrini, E., Lorenzini, G., Loppi, S., Nali, C., 2014. Evaluation of the suitability of *Tillandsia usneoides* (L.) L. As  
716 biomonitor of airborne elements in an urban area of Italy, Mediterranean basin. *Atmos. Pollut. Res.* 5, 226–  
717 235. <https://doi.org/10.5094/APR.2014.028>
- 718 Rahn, K. A., 1976. *The Chemical Composition of the Atmospheric Aerosol*. Graduate School of Oceanography,  
719 University of Rhode Island.
- 720 Reimann, C., De Caritat, P., 2005. Distinguishing between natural and anthropogenic sources for elements in the  
721 environment: Regional geochemical surveys versus enrichment factors. *Sci. Total Environ.* 337, 91–107.  
722 <https://doi.org/10.1016/j.scitotenv.2004.06.011>
- 723 Rochereau, F., Albinet, R., Labastie, A., Huron, Y., Vaxélaire, S., Rivet, F., Nedellec, J., 2021. Anciens sites miniers  
724 et industriels de la vallée de l'Orbiel (11) Rapport annuel de surveillance 2020. Rapp. Final BRGM BRGM/RP-  
725 71, 195.
- 726 Rudnick, R.L., Gao, S., 2003. Composition of the Continental Crust. *Treatise on Geochemistry* 3, 64.  
727 <https://doi.org/10.1016/B0-08-043751-6/03016-4>
- 728 Sánchez de la Campa, A.M., de la Rosa, J.D., Fernández-Caliani, J.C., González-Castanedo, Y., 2011. Impact of  
729 abandoned mine waste on atmospheric respirable particulate matter in the historic mining district of Rio  
730 Tinto (Iberian Pyrite Belt). *Environ. Res.* 111, 1018–1023. <https://doi.org/10.1016/j.envres.2011.07.001>
- 731 Schreck, E., Sarret, G., Oliva, P., Calas, A., Sobanska, S., Guédron, S., Barraza, F., Point, D., Huayta, C., Couture, R.,  
732 Prunier, J., Henry, M., Tisserand, D., Goix, S., Chincheros, J., Uzu, G., 2016. Is *Tillandsia capillaris* an efficient  
733 bioindicator of atmospheric metal and metalloid deposition ? Insights from five months of monitoring in  
734 an urban mining area. *Ecol. Indic.* 67, 227–237. <https://doi.org/10.1016/j.ecolind.2016.02.027>
- 735 Schreck, E., Viers, J., Blondet, I., Auda, Y., Macouin, M., Zouiten, C., Freydier, R., Dufrécho, G., Chmeleff, J.,  
736 Darrozes, J., 2020. *Tillandsia usneoides* as biomonitors of trace elements contents in the atmosphere of  
737 the mining district of Cartagena-La Unión (Spain): New insights for element transfer and pollution source  
738 tracing. *Chemosphere* 241. <https://doi.org/10.1016/j.chemosphere.2019.124955>

- 739 Tepanosyan, G., Sahakyan, L., Belyaeva, O., Asmaryan, S., Saghatelyan, A., 2018. Continuous impact of mining  
740 activities on soil heavy metals levels and human health. *Sci. Total Environ.* 639, 900–909.  
741 <https://doi.org/10.1016/j.scitotenv.2018.05.211>
- 742 Tomlinson, D.L., Wilson, J.G., Harris, C.R., Jeffrey, D.W., 1980. Problems in the assessment of heavy-metal levels  
743 in estuaries and the formation of a pollution index. *Helgoländer Meeresuntersuchungen* 33, 566–575.  
744 <https://doi.org/10.1007/BF02414780>
- 745 Trueb, L.F., 1996. The salsigne gold mine: A world-class ore body in the south west of France. *Gold Bull.* 29, 137–  
746 140. <https://doi.org/10.1007/BF03214749>
- 747 Vermeersch, F., Labebvre, O., Vachette, C., 2012. Exploitations minières sur le secteur de Salsigne. Concessions  
748 de Malabau, Pujol, Lastours, La Caunette, Salsigne, Villanière, Villardonnell . Evaluation et cartographie des  
749 aléas mouvements de terrain. *Rapp. synthèse Géoderis* 39.
- 750 Veysseyre, A., Moutard, K., Ferrari, C., Velde, K. Van de, Barbante, C., Cozzi, G., Capodaglio, G., Boutron, C., 2001.  
751 Heavy metals in fresh snow collected at different altitudes in the Chamonix and Maurienne valleys, French  
752 Alps: Initial results. *Atmos. Environ.* 35, 415–425. [https://doi.org/10.1016/S1352-2310\(00\)00125-4](https://doi.org/10.1016/S1352-2310(00)00125-4)
- 753 World Health Organization, 2021. WHO global air quality guidelines. Guidelines 1–360.
- 754 World Health Organization, 2016. Ambient air pollution: a global assessment of exposure and burden of disease.  
755 Rapport 1–131.
- 756 Yulevitch, G., Danon, M., Krasovitev, B., Fominykh, A., Swet, N., Tsesarsky, M., Katra, I., 2020. Evaluation of wind-  
757 induced dust-PM emission from unpaved roads varying in silt content by experimental results. *Atmos.*  
758 *Pollut. Res.* 11, 261–268. <https://doi.org/10.1016/j.apr.2019.10.010>
- 759 Zota, A.R., Willis, R., Jim, R., Norris, G.A., Shine, J.P., Duvall, R.M., Schaidler, L.A., Spengler, J.D., 2009. Impact of  
760 mine waste on airborne respirable particulates in Northeastern Oklahoma, United States. *J. Air Waste*  
761 *Manag. Assoc.* 59, 1347–1357. <https://doi.org/10.3155/1047-3289.59.11.1347>
- 762